Optimizing and upscaling of USP laser structuring for 3D lithium-ion battery electrodes for fast-charging and reduced lithium plating

Y. Sterzl[a,*], M. Pulst[b], S. Xiao[c], C. Franke[d], W. Pfleging[a]
[a]Institute for Applied Materials, Karlsruhe Institute of Technology, Karlsruhe, Germany
[b]EAS Batteries GmbH, Nordhausen, Germany
[c]EdgeWave GmbH, Würselen, Germany
[d]n2-Photonics GmbH, Hamburg, Germany

ABSTRACT

Various concepts for upscaling the laser structuring of electrodes for lithium-ion batteries are studied on commercial lithium-iron-phosphate electrodes. Attention was paid to the thermal modifications of the active material due to high power laser material processing. Therefore, the influence of ultrashort pulse widths in the range of 220 fs were compared to the ablation with pulse widths in the range of 600 fs. The realization of the ultrashort pulses was achieved through self-phase modulation based spectral broadening and subsequent pulse compression via chirped mirrors. Furthermore, the influence of GHz pulse burst ablation on ablation efficiency was studied for varying pulse burst lengths from 50 ns to 500 ns. The ablation result of the lithium-iron-phosphate electrodes with various pulse width and pulse bursts were evaluated in terms of processing quality and compared to single pulse ablation. In addition, fast-charging capability of full cells with all possible combinations of structured and unstructured electrodes were examined in a charge and discharge rate capability test, differential voltage analysis of the voltage relaxation, and post-mortem studies to examine the fast-charging capability and lithium plating behavior.

Keywords: ultrashort pulsed laser ablation, fast-charging, lithium-ion battery, 3D battery, upscaling, electrode structuring, GHz burst ablation

1. INTRODUCTION

Batteries of high energy density, power density, safety, and service life are needed to supply the increasing electrification of the transportation sector with energy storage systems. Therefore, the consistent further development of lithium-ion batteries (LIB), especially in terms of fast-charging remains a key factor [1]. One way to increase the fast-charging and discharging capability and lifetime of the later battery at the electrode level is the modification of the electrode architecture, either by mechanical or laser ablation, additive manufacturing, or multilayer coating [2-5]. A modification of the electrode architecture, e.g., implementing a material gradient, porosity gradients or microstructures into the electrode, leads to a reduced effective tortuosity in the electrode and with that to a decreased Li-ion diffusion overpotential [6]. The advantage of ablative structuring of electrodes compared to modifying the electrode architecture using additive manufacturing or multilayer coating is that it can be integrated into existing production lines without having to change the electrode chemistry [7]. Furthermore, it was shown that the mechanical stability of the electrode coating during winding, as occurs in the production of cylindrical cells, can be increased by suitable structuring of electrodes with line structures, which leads to smaller possible winding radii and thus also to an increase in the achievable energy density of the subsequent battery cell [8]. To realize integration of the laser structuring in an industrial electrode manufacturing environment, however, the structuring process speed must be able to keep pace with the remaining process steps to not limit the processing speed of electrode production. The achievable processing speed for laser structuring is a function of the electrode band width, the structure pattern, and the structure pitch, as well as the laser process parameters such as the required pulse peak fluence, and the number of laser scans for the targeted ablation depth and the used scanning speed [9, 10]. It has been shown in the case of graphite and silicon graphite electrodes that the laser structuring of these electrodes with ultrashort pulsed (USP) lasers requires laser powers in the range of several kW [9]. Simply increasing the pulse peak fluence to increase the ablation rate is only of limited use, as it has been shown that increasing the pulse peak fluence also increases the ablation width of the structures and thus the mass loss through structuring due to a higher ablation volume [9, 10]. In order to further increase the ablation efficiency, the use of pulse bursts in the MHz range was recently investigated for the structuring of various electrode materials and an increase in the removal rate by a factor of 2.5 to 5 was found for LFP or NMC electrodes [11, 12]. Nevertheless, attention must be paid to the choice of laser process parameters, as active materials such as LFP or NMC show thermally-driven material modifications at high pulse peak fluences, high repetition rates, or pulse widths in the ns-

regime, which can later have a negative impact on the electrochemical performance and need to be counteracted using ultrashort laser pulses and appropriate processing parameters [13].

The work presented here focuses on the laser structuring of LFP electrodes. The influence of GHz pulse burst ablation and the influence of the pulse width in case of single pulse ablation was studied regarding the ablation characteristic and possible thermal modifications of the electrode material. In order to achieve pulse widths shorter than 600 fs, the laser was coupled into a commercial nonlinear pulse compression setup to reach a compressed output pulse duration of 220 fs. With that, suitable process windows for laser structuring of commercial LFP and graphite electrodes are defined. Furthermore, the electrochemical performance of full cells with LFP cathodes and graphite anodes, in all possible combinations of structured and unstructured electrodes, were investigated in a discharge and charge rate capability test, differential voltage analysis of the voltage relaxation and post-mortem studies to investigate the lithium plating behavior. This allowed to define suitable pairing combinations of structured and unstructured anodes and cathodes, so that the electrode structuring can later be tuned to the required application profile.

2. EXPERIMENTAL

Laser structuring and electrode characterization

In order to investigate the influence of the pulse width on the ablation of commercial LFP electrodes (EAS Batteries GmbH, Nordhausen, Germany), a high power and high repetition rate laser system (FX, EdgeWave GmbH, Würselen, Germany) with a pulse width of 600 fs operating at a wavelength of 1030 nm and a maximum average power of >300 W was implemented in an optical setup consisting of a beam expender with a magnification factor of 3, and a F-theta lens with a focus length of 100 mm. To further decrease the pulse width, the laser was coupled into a commercial nonlinear pulse compression setup (MIKS1_S, n2-Photonics GmbH, Hamburg, Germany). Inside the unit the laser pulse spectrum was broadened via self-phase modulation in an argon-filled multi-pass cell and subsequently compressed via an integrated set of chirped mirrors. Additional chirped mirrors outside the module were used to fine-tune the dispersion compensation and reach a compressed output pulse duration of 220 fs.

The LFP electrodes were structured at a repetition rate of 1.5 MHz, a scanning speed of 20 m s^{-1}, two pulse energies of 26.67 µJ and 40 µJ, and with increasing number of laser scan passes ranging from 3 to 27. The ablation results were examined regarding possible visible material modifications on the electrode surface in a scanning electron microscope (SEM. Phenom Pro, Thermo Fisher Scientific, Waltham, MA, USA).

The influence of pulse burst ablation on LFP electrodes (EAS Batteries GmbH, Nordhausen, Germany) was studied with a high power and high repetition rate laser system (PXpv, Edgewave GmbH, Würselen, Germany) with an intra-pulse width of 10 ps operating at a wavelength of 1064 nm, and a maximum average power of 440 W. The number of pulses per burst (PPB) is adjustable from 20 to 500 which corresponds to a burst length of 20 ns to 500 ns due to the fixed repetition rate in the burst ($f_{rep,B}$) of 1 GHz. Figure 1 shows schematically the differences between pulse burst ablation and single pulse ablation.

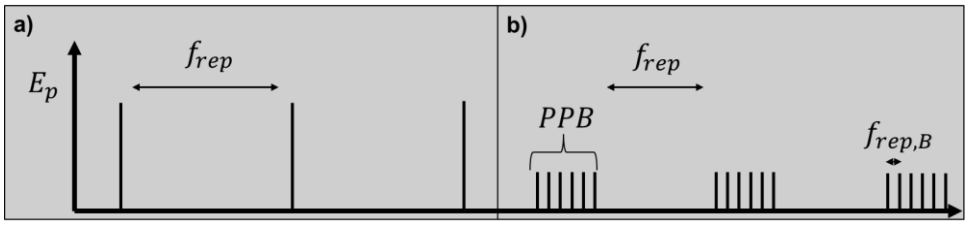

Figure 1. Example of operation without (a) and with pulse burst mode (b).

The laser was implemented in a laser processing unit (MSV203 Laser Patterning Tool, M-SOLV LTD, Oxford, UK). Single pulse ablation experiments were performed using a high-power laser (FX, EdgeWave GmbH, Würselen, Germany) operating at a wavelength of 1030 nm and a pulse width of 600 fs, implemented in the same laser processing unit. All used lasers in the experimental setups with variation of the pulse width and burst ablation are listed in Table 1.

Table 1. Specifications of all the setups used for electrode structuring in this work.

Setup	reference	GHz-burst	pulse compression	reference pulse compression
Wavelength	1030 nm	1064 nm	1030 nm	1030 nm
Pulse width	600 fs	10 ps	220 fs	600 fs
Av. focus diameter	23 µm	23 µm	17 µm	17 µm

Commercial LFP electrodes were structured at a repetition rate of 150 kHz, a laser scanning speed of 2 m s^{-1}, and average powers of 2 W to 8 W. In case of the GHz burst ablation, the PPB were set to 50 and 500. The structures were examined in terms of thermally driven material modification by SEM (Phenom Pro, Thermo Fisher Scientific, Waltham, MA, USA). The ablation characteristic of the laser generated structures was examined via focus variation using a digital microscope (VHX7000, KEYENCE, Osaka, Japan). The analyzed profiles represent an average of 21 profiles at pitch distance of 20 µm. The profiles of the structures were further analyzed by computational peak analysis (OriginPro 2022, OriginLab Corporation, Northampton, MA, USA) in terms of ablation depth and width. Cross-section analysis of the structured electrodes with an optical microscope (Reicher-Jung MeF3, Leica Microsystems, Wetzlar, Germany) was used to validate the results of focus variation.
The electrodes for the electrochemical characterization were structured with a line pattern using the reference setup described above, with the exemption, that the laser was set to MHz-burst ablation mode with a PPB of 6, a $f_{rep,B}$ of 50 MHz, a f_{rep} of 1.5 MHz, a scanning speed of 20 m s^{-1}, an average laser power of 50 W and a sufficient number of laser passes to achieve an ablation depth close to the coating thickness.

Electrochemical characterization

All possible combinations of full cells with structured and unstructured electrodes were investigated, i.e., full cells with tructured cathode and unstructured anode ($A_{us}C_s$), structured anode and unstructured cathode (A_sC_{us}), structured anode and cathode (A_sC_s) and unstructured anode and cathode ($A_{us}C_{us}$). To ensure comparability of the respective combinations, graphite anodes and LFP cathodes with two different mass loadings were used to compensate for the mass loss due to structuring. The structure pitch was set to 300 µm in case of the anodes and 150 µm in case of the cathodes. The areal capacities of the used electrodes are listed in Table 2.

Table 2. Specification of the built full cells with combinations of structured (s) and unstructured (us) anodes (A) and cathodes (C).

Full cell	$A_{us}C_{us}$	A_sC_{us}	$A_{us}C_s$	A_sC_s
Areal capacity (anode/cathode)	3.5 mAh cm^{-2}/ 3.2 mAh cm^{-2}	3.3 mAh cm^{-2}/ 3.2 mAh cm^{-2}	3.5 mAh cm^{-2}/ 3.1 mAh cm^{-2}	3.3 mAh cm^{-2}/ 3.1 mAh cm^{-2}

One coating of the double-sided coated electrodes was removed by laser ablation, so that the electrodes could be assembled in coin cells in CR2032 format. Cathodes with a diameter of 12 mm and anodes with a diameter of 15 mm were laser cut and subsequently dried in a vacuum oven at 100 °C for 24 h to remove excess moisture. CR2032 coin cells were assembled in an argon-filled glove box (LAB master pro sp, M. Braun Intergas-Systeme GmbH, Garching, Germany). Each full cell was constructed of one anode and cathode, electrolyte (1M $LiPF_6$ salt in a solvent mixture of ethylene, ethyl methyl carbonate, and dimethhyl carbonate with 2 wt.% VC additive), and a 25 µm polypropylene (PP) separator. The cells were stored for 20 h at 20°C prior to formation to ensure a homogeneous wetting of the electrodes and separator with liquid electrolyte. Galvanostatic cycling with potential limitations (GCPL) was performed using a battery cycler (LBT, Arbin Instruments, College Station, TX, USA). The formation consisted of constant current (CC) charging at a C-rate of 0.025C to a cut of voltage of 3.6 V with subsequent constant voltage (CV) charging until the current drops to an equivalent of 0.0125C followed by CC discharging at 0.025C to a voltage of 2.5 V. Between every charging and discharging step a rest phase of 15 min was implemented. The formation followed a discharge rate capability and charge rate capability test shown in Table 3 and Table 4. For the charge rate capability test, the CV step of every forth cycle was additionally limited in time (15 min). The CV step of these cycles was followed by a rest phase of 4 hours to analyze the voltage relaxation.

Table 3. Protocol of the discharge rate capability test.

Charging (CC)	0.2C	0.5C	0.5C	0.5C	0.5C	0.5C	0.5C	0.5C	0.2C
Cut off current (CV)	0.025C	0.025C	0.025C	0.025C	0.025C	0.025C	0.025C	0.025C	0.025C
Discharge (CC)	0.2C	0.5C	1C	2C	3C	5C	10C	15C	0.2C
Cycles	3	3	3	3	3	3	3	3	3

Table 4. Protocol of the charge rate capability test.

Charging (CC)	0.5C	1C	2C	3C	5C	0.2C
Cut off current (CV)	0.025C	0.025C	0.025C	0.025C	0.025C	0.025C
Discharge (CC)	0.5C	0.5C	0.5C	0.5C	0.5C	0.2C
Cycles	4	4	4	4	4	4

3. RESULTS AND DISCUSSION

Influence of the pulse width on the ablation of LFP electrodes

Thermally induced modifications of the LFP active material due to laser structuring have also been shown using ultrashort pulses of 600 fs, by using high pulse peak fluences of 33 J cm^{-2} and repetition rates of 1.5 MHz [8]. Although a moderate amount of visible thermal modification of structured LFP electrodes did not show any disadvantages regarding the achievable specific capacity, the consequences for the long-term stability are still unclear and any form of thermal modification of the active material should be avoided [8]. Therefore, the integration of a pulse compressor was investigated in this study to further reduce the pulse width from 600 fs to 220 fs and thus further reduce a possible thermal impact even at high repetition rates and pulse peak fluences. Figure 2 shows the differences in ablation characteristics and surface topography for the laser structuring of LFP electrodes with an average laser power of 60 W (Figure 2a, b), and 40 W (Figure 2c, d), a scanning speed of 20 m s^{-1} and a number of 24 laser scan passes with (Figure 2a, c) and without (Figure 2b, d) reduced pulse width to 220 fs. While a significant reduction in the ablation width was observed for both laser powers with a decreasing pulse width to 220 fs, the shorter pulse widths did not lead to a reduction in the visible thermal modifications on the groove sidewalls.

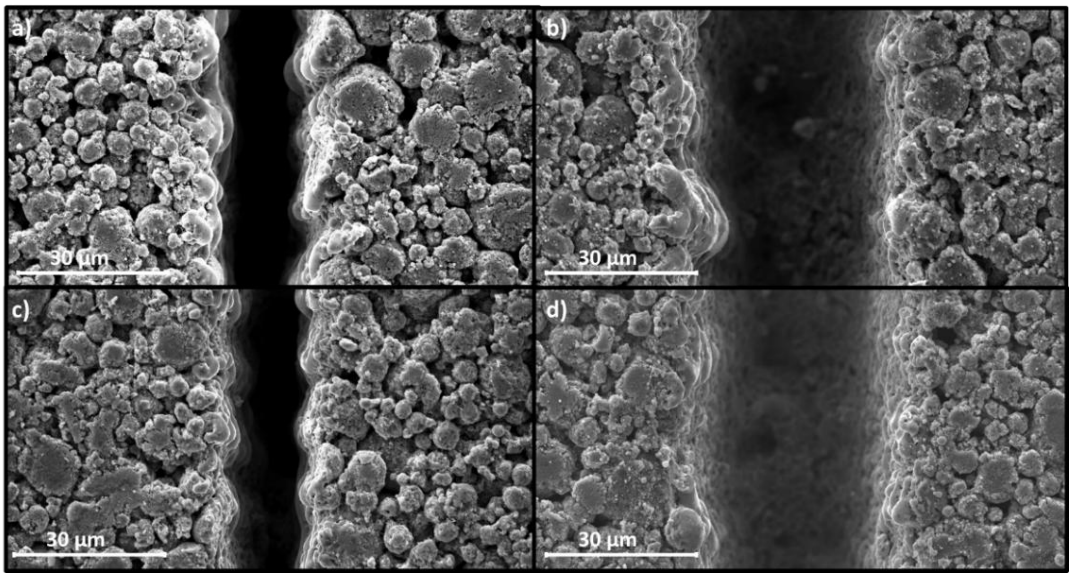

Figure 2. Top view SEM images of LFP cathodes structured at 60 W, 1.5 MHz, 20 m s^{-1}, and 24 laser scan passes (a, b) and 40 W, 1.5 MHz and 20 m s^{-1} and 24 laser scan passes (c, d) with pulse compression to 220 fs (a, c) and without pulse compression (b, d).

The inspection of the top view SEM images shows that there tend to be larger areas of material modifications on the side walls of the grooves structured at 220 fs compared to the grooves structured at 600fs. The higher aspect ratio of the grooves structured at a pulse width of 220 fs due to the reduced width compared to the grooves structured at a pulse width of 600 fs indicates that the modifications could be caused by the interaction of laser-induced material vapor plasma with the groove sidewalls, instead of laser-induced heat accumulation. If this is the case, the modifications should become more pronounced with an increasing number of passes, as the aspect ratio of the grooves increases with increasing ablation depth and the laser-induced material vapor plasma can then interact with the side walls. Figure 3 shows top view SEM images of a LFP electrode structured with 3, 12, and 18 laser scan passes with (Figure 3a, b, c) and without pulse compression (Figure 3d, e, f). In both cases, thermal modification of the active material are not visible up to 12 laser scan passes (Figure 3b, e), and get more pronounced from 18 laser scan passes until they are clearly visible at 24 laser scan passes in Figure 2.

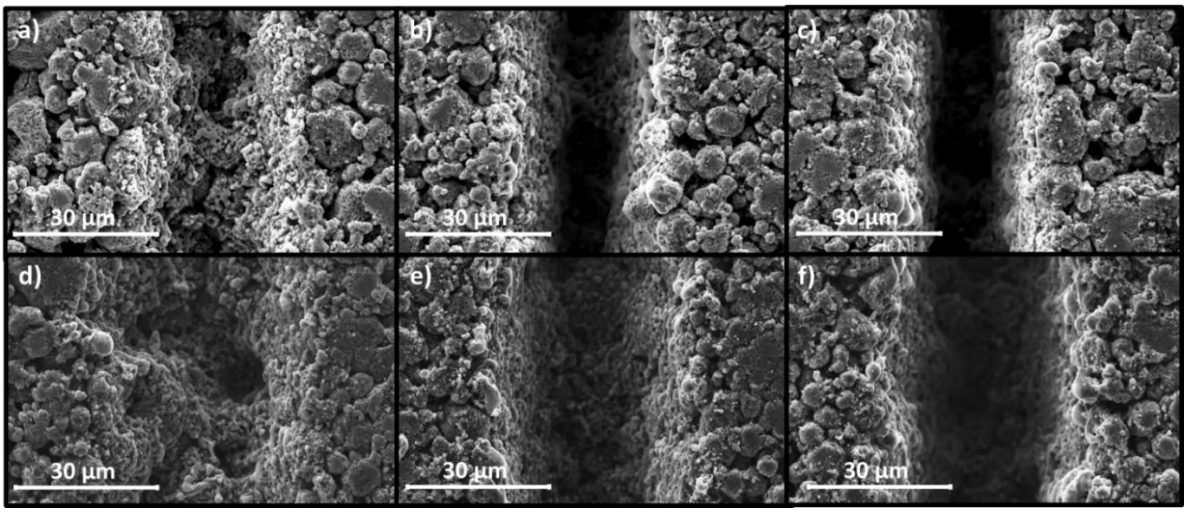

Figure 3. Top view SEM images of LFP cathodes structured at 60 W, 1.5 MHz, 20 m s^{-1}, with (a, b, c) and without (d, e, f) pulse compression and 6 (a, d), 12 (b, e) and 18 (c, f) laser scan passes.

GHz ablation of LFP electrodes

For industrial-like electrode production, a trade-off must be found between the structure quality and the achievable processing speed. Efforts are therefore being made to increase the ablation efficiency. The investment costs regarding the laser beam source and the availability of laser beam sources with sufficient power must also be considered. The ablation volume is less suitable as a target for determining parameters to increase ablation efficiency, as narrow grooves with a high aspect ratio are aimed for, since the ablation width significantly determines the mass loss. The aim of a comparative study between different laser sources is therefore to achieve the highest possible ablation depth at similar pulse peak fluence and at the same time a small ablation width with acceptable thermal modifications to the active material. In the case of burst ablation, a comparison can be made with single-pulse ablation by comparing the ablation result at a similar single-pulse peak fluence, which in the case of burst ablation is the peak fluence of the individual pulses in the burst, or a burst fluence, which is the sum of the peak fluence of the individual pulses in the burst. A comparison with the same burst fluence and pulse peak fluence is useful, as different foci are taken into account for different optical setups and, in the case of similar foci sizes, the energy input into the material is similar, which allows a direct efficiency evaluation. In Figure 4 the ablation depth (Figure 4a) and width (Figure 4b) after three laser scanning passes structured at a f_{rep} of 150 kHz and a scanning speed of 2 m s^{-1} are shown. The use of a longer burst length of 500 ns leads to an increase in the ablation depth at burst fluences higher 20 J cm^{-2} compared to bursts with a length of 50 ns. Comparing GHz-burst ablation to single pulse ablation with 600 fs pulse and similar pulse peak fluence, the ablation depth is increased by a factor of 2. If the ablation width is examined as a function of the burst fluence or pulse peak fluence, it can be seen that the widest grooves are ablated with single-pulse ablation with a pulse width of 600 fs, while the narrowest grooves with an ablation in the range of 15 µm to 20 µm are ablated with GHz-burst ablation. In the examination of the top view SEM images (not shown here) of the ablation at 20 J cm^{-2} burst fluence or pulse peak fluence, thermal modifications of the active material were evident for GHz-burst ablation, while no significant changes were observed on the groove sidewalls with single pulse ablation at 600 fs.

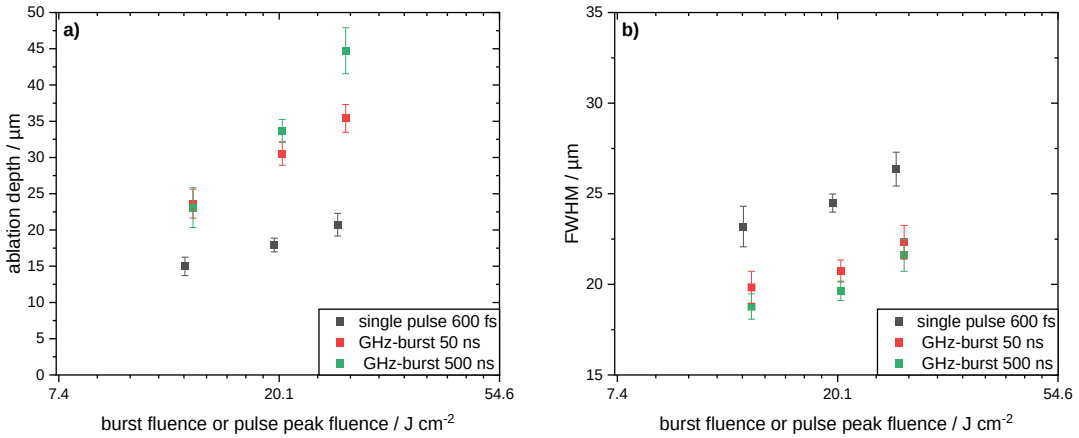

Figure 4. Ablation depth (a) and ablation width (b) as a function of pulse peak or burst fluence for LFP electrodes, structured at 150 kHz, 2 m s^{-1}, and 3 laser scan passes.

Fast charging and discharging capability

Battery cell performance can be defined by their fast-charging and -discharging rate capability. In terms of process upscaling of the 3D battery concept, it is necessary to identify whether a structuring of anode and cathode or only of anode or cathode in the corresponding application scope is suitable, since the latter would lead to an increase in process speed. Figure 5 shows the discharge (Figure 5a) and the charge (Figure 5b) rate capability test of the test protocols listed in Table 3 and Table 4. For both the charging and discharging, the cells with structured anodes and cathodes reached the highest capacities at C-rate higher 2C. Cells with a structured cathode and unstructured anode showed higher capacities with increasing C-rate in both the charge and discharge rate capability test compared to cells with a structured anode and unstructured cathode. The lowest capacities in the charging rate capability test are measured in cells with an unstructured anode and cathode. When considering the charging rate capability test, however, it must be considered that possible lithium plating during charging at high C-rates is also measured as capacity. For this reason, the coulombic efficiency or voltage relaxation after charging should be examined to detect possible undesired lithium plating [6, 14, 15].

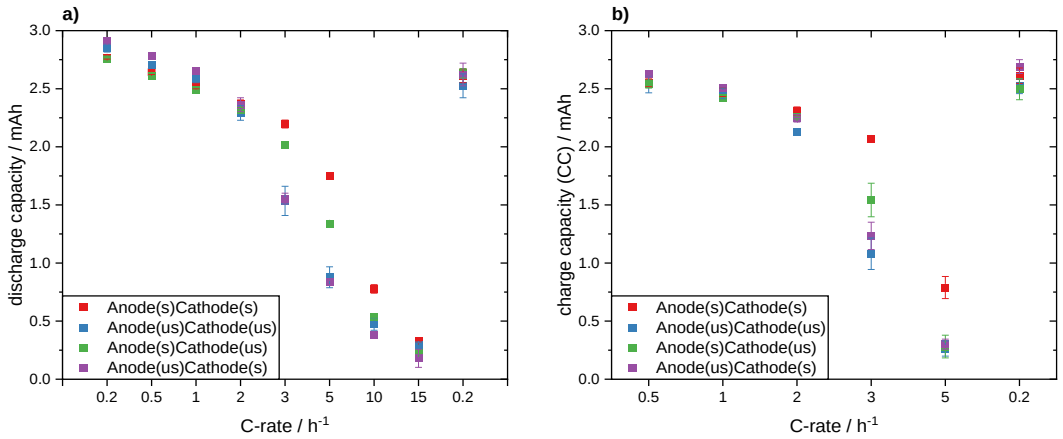

Figure 5. Discharge (a) and charge (b) rate capability test of graphite/LFP full cells with structured (s) and unstructured (us) electrode combinations.

Figure 6 shows the voltage relaxation (Figure 6, dotted line) and dV/dt (Figure 6, solid line) plot after each 4th cycle of fast charging, of one representative cell of each electrode pairing. No peak in the dV/dt is observed for all electrode pairings

up to 2C fast charging. The unstructured electrode pairing showed plaiting according to the dV/dt analysis after 3C charging, while all other electrode combinations except of the structured anode and cathode combination, showed a peak in the dV/dt after 5C charging. Regarding to a fast charging with avoiding of lithium plaiting, the structuring of both electrodes seems to be beneficial. Furthermore, if one examines the peak width, which is also an indicator for the amount of plated lithium, the structuring of the anode seems to more beneficial compared to a structuring of the cathode [16]. This is also evident in the post-mortem analysis of the anode after charging, in which large areas of plated lithium could be found on unstructured anodes, whereas in the case of structured anodes only small areas of plated lithium were present (not shown here). These results should be taken into account by ranking the charging rate capability tests shown in Figure 5b.

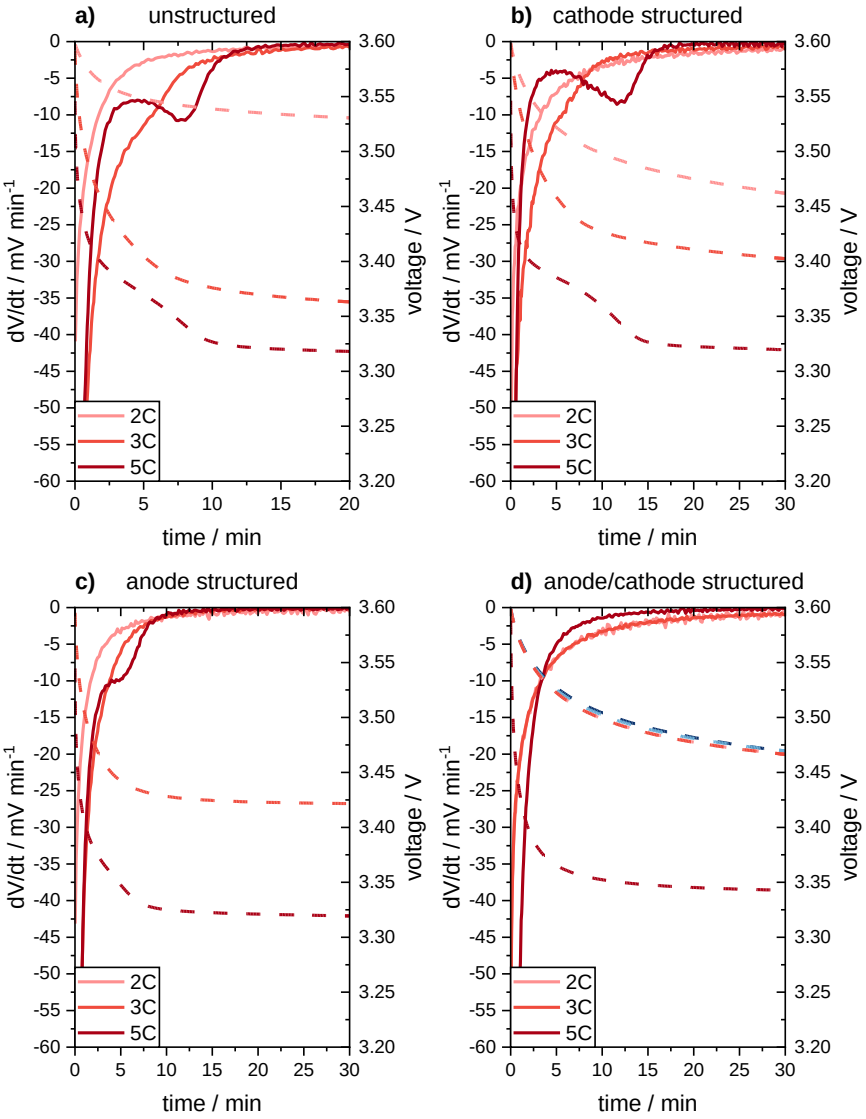

Figure 6. Voltage relaxation analysis (dotted line) and dV/dt analysis (solid line) after each 4th cycle of the charge rate capability test of one representative cell of all studied electrode combinations.

4. CONCLUSION AND OUTLOOK

In this study the influence of USP laser ablation, with pulse widths in the range of 220 fs and 600 fs on LFP electrodes were examined. A reduction in the visible amount of laser-induced modifications of the active material after structuring at high power (60 W) and high repetition rates (1.5 MHz) was not observed for a reduction of pulse width from 600 fs down to 220 fs. The development of the extent of the thermal modifications as a function of the number of passes indicates that the modifications are not induced by heat accumulation, but rather by the interaction of the resulting material vapor plasma with the side walls of the electrode. However, a reduction of the pulse width is advantageous regarding the aspect ratio of the laser generated structures. This at the end reduces the mass loss due to structuring and decreases the later costs of electrode production. To further increase the laser processing speed to match the belt speed of electrode coating, the use of ps GHz burst ablation on LFP electrodes was examined. It could be shown that by using GHz burst ablation with PPB of 50-500, the ablation rate could be increased up to a factor of 2 compared to single pulse fs ablation. Furthermore, the ablation width was also decreased by the use of GHz burst ablation, leading to high aspect ratio structures in the electrode. However, in the case of GHz ablation, the SEM analysis revealed modifications of the active material, which were not visible with single pulse fs ablation using the same parameters. The electrochemical characterization of batteries with all possible structured and unstructured electrodes combinations showed, that cells with a combination of a structured anode and structured cathode reached the highest capacities in the discharge and the charge rate capability test. Cells with only a structured cathode showed the second-highest capacities in the discharging and charging rate capability test. However, the voltage relaxation analysis and the post-mortem examination after charging showed that the structuring of the anode is advantageous with regard to lithium plating. The results of the charge rate capability test must therefore be critically reviewed, as lithium plating during charging is also incorrectly measured as capacity in this case.

ACKNOWLEDGEMENTS

We are grateful to our colleagues Marek Kapitz and Alexandra Reif for their support during laser processing and analytics. This project has received funding from Federal Ministry of Education and Research (BMBF, High-E-Life, 03XP0495).

REFERENCES

[1] M. Weiss, R. Ruess, J. Kasnatscheew *et al.*, “Fast Charging of Lithium-Ion Batteries: A Review of Materials Aspects,” Advanced Energy Materials, 11(33), (2021).

[2] W. Pfleging, “Recent progress in laser texturing of battery materials: a review of tuning electrochemical performances, related material development, and prospects for large-scale manufacturing,” International Journal of Extreme Manufacturing, 3(1), (2020).

[3] U. Rist, V. Falkowski, and W. Pfleging, “Electrochemical Properties of Laser-Printed Multilayer Anodes for Lithium-Ion Batteries,” Nanomaterials (Basel), 13(17), (2023).

[4] J. Keilhofer, L. W. F. Schaffranka, A. Wuttke *et al.*, “Mechanical Structuring of Lithium-Ion Battery Electrodes Using an Embossing Roller,” Energy Technology, 11(5), (2023).

[5] L. Gottschalk, C. Oertel, N. Strzelczyk *et al.*, “Improving the Performance of Lithium-Ion Batteries Using a Two-Layer, Hard Carbon-Containing Silicon Anode for Use in High-Energy Electrodes,” Energy Technology, 11(5), (2022).

[6] K.-H. Chen, M. J. Namkoong, V. Goel *et al.*, “Efficient fast-charging of lithium-ion batteries enabled by laser-patterned three-dimensional graphite anode architectures,” Journal of Power Sources, 471, (2020).

[7] L. Hille, M. P. Noecker, B. Ko *et al.*, “Integration of laser structuring into the electrode manufacturing process chain for lithium-ion batteries,” Journal of Power Sources, 556, (2023).

[8] Y. Sterzl, S. Xiao, M. Pulst *et al.*, “Addressing Mechanical and Electrochemical Aging of Cylindrical LFP Battery Cells by Laser Structuring of Electrodes,” 2024 IEEE International Conference on Manipulation, Manufacturing and Measurement on the Nanoscale (3M-NANO), 223-227 (2024).

[9] A. Meyer, Y. Sterzl, and W. Pfleging, “High repetition ultrafast laser ablation of graphite and silicon/graphite composite electrodes for lithium-ion batteries,” Journal of Laser Applications, 35(4), (2023).

[10] Y. Sterzl, and W. Pfleging, “Extending the 3D-battery concept: large areal ultrashort pulsed laser structuring of multilayered electrode coatings,” Proc. of SPIE, 12409, 9 (2023).

[11] A. Sikora, L. Gemini, M. Faucon *et al.*, “Benefits of Femtosecond Laser 40 MHz Burst Mode for Li-Ion Battery Electrode Structuring,” Materials (Basel), 17(4), (2024).

[12] M. Trenn, T. Keller, K. Voigt *et al.*, “Efficiency enhancement of Li-ion battery electrode structuring by pulse burst processing: results of an automated study,” Proc. SPIE, 12873, (2024).
[13] M. Mangang, H. J. Seifert, and W. Pfleging, “Influence of laser pulse duration on the electrochemical performance of laser structured LiFePO4 composite electrodes,” Journal of Power Sources, 304, 24-32 (2016).
[14] C. Uhlmann, J. Illig, M. Ender *et al.*, “In situ detection of lithium metal plating on graphite in experimental cells,” Journal of Power Sources, 279, 428-438 (2015).
[15] Z. M. Konz, E. J. McShane, and B. D. McCloskey, “Detecting the Onset of Lithium Plating and Monitoring Fast Charging Performance with Voltage Relaxation,” ACS Energy Letters, 5(6), 1750-1757 (2020).
[16] C. von Lüders, V. Zinth, S. V. Erhard *et al.*, “Lithium plating in lithium-ion batteries investigated by voltage relaxation and in situ neutron diffraction,” Journal of Power Sources, 342, 17-23 (2017).